Mass budgets of the Lambert, Mellor and Fisher glaciers and basal fluxes beneath their flowbands on Amery Ice Shelf

Jiahong Wen[1, 2], Kenneth C. Jezek[2], Helen A. Fricker[3], Beata M. Csatho[2], Ute C. Herzfeld[4], Katy L. Farness[2], Philippe Huybrechts[5, 6]

[1]*Department of Geography, Shanghai Normal University, Shanghai 200234, China*
[2]*Byrd Polar Research Center, The Ohio State University, Columbus, OH 43210, USA*
[3]*IGPP, Scripps Institution of Oceanography, University of California San Diego, La Jolla, CA 92093-0225, USA*
[4] *CIRES/NSIDC, University of Colorado Boulder, Boulder, CO 80309-0449, USA*
[5]*Departement Geografie, Vrije Universiteit Brussel, Pleinlaan 2, B-1050, Brussels, Belgium*
[6]*Alfred-Wegener-Institut für Polar- und Meeresforschung, Postfach 120161, D-27515 Bremerhaven*

Abstract. We use in situ measurements and remote-sensing data sets to evaluate the mass budgets of the Lambert, Mellor and Fisher glaciers and the basal melting and freezing beneath their flowbands on the Amery Ice Shelf. Lambert and Mellor glaciers upstream the ANARE LGB traverse have positive imbalances of 3.9±2.1 Gt a^{-1} and 2.1±2.4 Gt a^{-1} respectively while the Fisher Glacier is approximately in balance. The upstream region as a whole has a positive imbalance of 5.9±4.9 Gt a^{-1}. The three glaciers downstream the traverse line are in negative imbalance, and the whole downstream region has a negative imbalance of -8.5±5.8 Gt a^{-1}. The mass budgets of the Lambert, Mellor, and Fisher glaciers are close to balance. The whole drainage basin of the three glaciers is also approximately in balance with a mass budget of -2.6±6.5 Gt a^{-1}. The significant positive imbalances for the interior basin upstream the GL line reported previously are possibly due to overestimate of the total accumulation and underestimate of the ice flux through the GL line.

The mean melting rate is -23.0±3.5 m ice a^{-1} near the southern grounding line, which decreases rapidly downstream, and transits to refreezing at around 300 km from the southern extremity of the shelf. Freezing rates of the flowbands are around 0.5±0.1 to 1.5±0.2 m ice a^{-1}. The percentage of the loss of the ice from interior by basal melting beneath the flowbands is about 80±5%. The total basal melting, refreezing beneath the three flowbands are 50.3±5.0 Gt ice a^{-1} and 7.0±0.7 Gt ice a^{-1} respectively. The total basal melting and net melting are much larger than the results for the whole Amery Ice Shelf

derived from modeling and oceanographic data from Prydz Bay.

1 Introduction

The Antarctic Ice sheet holds approximately 90% of the ice in the world so that only a small imbalance between snowfall and discharge of ice and meltwater into the ocean could significantly alter global sea level. Measurement and assessment of Antarctic Ice sheet mass balance are of keen interest to Antarctic research community. Many authors have made estimates of the mass balance of the entire ice sheet (e.g., Bentley and Giovinetto, 1991; Jacobs *et al.*, 1992; Rignot and Thomas, 2002) as well as individual drainage systems (e.g., Whillans and Bindschadler, 1988; Berthier *et al.*, 2003). However, the determination of growth or shrinkage of the great ice sheet is a longstanding unsolved scientific problem (The ISMASS Committee, 2004). Meanwhile, much of the coastline of Antarctica is fringed by floating ice shelves. The basal flux beneath the 1.6×10^6 km^2 floating portion of the Antarctic Ice Sheet (Jacobs *et al.*, 1996), resulted from the ice shelf-ocean interaction, is not only an important component of the Antarctic mass budget, but also a key factor to modification of the characteristics of the ocean and a significant contributor to the Antarctic Bottom Water formation. Studies (Jacobs *et al.*, 1996; Rignot and Jacobs, 2002) indicated that rapid bottom melting was widespread near Antarctic Ice Sheet grounding lines, and ice shelf net basal melting may account for up to one third of the loss from the floating ice. The basal flux beneath the ice shelves is probably still the least well know element of the Antarctic mass budget though remarkable advances have been achieved since Jenkins and Doake (1991) studied ice-ocean interaction on the Ronne Ice Shelf by means of detailed glaciological measurements.

Recent advances in remote sensing (particularly laser altimetry, radar altimetry, interferometric synthetic-aperture radar (InSAR), and Global Positioning System (GPS)) have resulted in a significant increase in our ability to estimate the mass balance of polar ice sheets. InSAR has been used to measure glacier velocities and map grounding-line position (Gray *et al.*, 2002; Joughin and Tulaczyk, 2002; Rignot, 2002); radar and laser altimetry have been applied to map the topography of the ice sheet unprecedented in terms of spatial extent and accuracy (Liu *et al.*, 1999; Zwally *et al.*; 2002; Herzfeld,

2004). This allowed us to obtain a more precise estimate of the mass budgets of the ice sheet and basal fluxes over beneath the ice shelf using standard glaciological methods combined with other data sets (Rignot and Thomas, 2002; Joughin and Padman, 2003), such as snow accumulation (Vaughan *et al.*, 1999; Giovinetto and Zwally, 2000) and ice thickness (Lythe *et al.*, 2001) compilations. Here we present a study of the mass budgets of the Lambert, Mellor and Fisher glaciers, upstream and downstream of the ANARE (Australian Antarctic Expedition) LGB traverse, and melting and freezing beneath the flowbands originating from those glaciers, using GIS (geographic information system) to combine a variety of data sets derived from in situ measurements and remote sensing data sets.

2 Study Area

Our study area covers the central part of the Lambert Glacier-Amery Ice Shelf system (hereafter, LAS), East Antarctica (Fig.1). We use the Fricker *et al.* (2000a, b) definition of the LAS, but the front of the Amery Ice shelf is defined by the RAMP (RADARSAT-1 Antarctic Mapping Project) image mosaic (Jezek, 1999). Located at 68.5-81ºS, 40-95ºE, it is the largest glacier-ice-shelf system in East Antarctica, and an important drainage basin in terms of the overall mass balance of Antarctica (Fricker *et al.*, 2000b). The grounded portion of our study area corresponds to the drainage basin of Lambert Glacier defined by Rignot (2002), which contains the three glaciers draining into the rear of the Amery Ice Shelf.

Defined by Allison (1979), The Lambert Glacier, fed by its three tributaries (the Lambert, Mellor and Fisher glaciers), is previously thought the largest grounded ice stream in the world. However, Fricker *et al.* (2002a) and Rignot (2002) showed that the grounding-line position of the Lambert Glacier was located much further south (up to around 240 km) than the previously reported position (Budd *et al.*, 1982), based on hydrostatic equilibrium and InSAR data. The newly determined grounding line is located at the zone of confluence of tributaries Lambert, Mellor and Fisher glaciers. It means the grounded Lambert Glacier previously thought is, in fact, a portion of the Amery Ice Shelf and the flowbands of its nourishing tributaries, and hereafter the Lambert Glacier used in

this study refers to as the tributary Lambert Glacier.

Figure 1

In an Arc/Info environment, the margin of the LAS was defined by the OSU digital elevation model (DEM) (Liu *et al.*, 1999). The grounding line of the Lambert, Mellor and Fisher glaciers (the southern grounding line), mapped interferometrically by Rignot (2002), is used in this study. The resulting precision of grounding-line mapping is 100 m for Lambert Glacier and 300 m for Mellor and Fisher glaciers (Rignot, 2002). The boundaries of the three glaciers are delineated by tracing the flow stripes, or foliation trends (Hambrey and Dowdeswell, 1994) derived from RAMP mosaic (Wu and Jezek, 2004) in the lower elevation portion (lower than around 2000-2500 m), and then tracing the steepest paths generated from OSU-DEM 5km triangular irregular network surface. The upstream and downstream drainages of these glaciers are defined by the ANARE LGB traverse line (Fig. 1).

Figure 2

Velocity in vector form with a spacing interval of 2 by 2 km derived from the Modified Antarctic Mapping Mission (MAMM) InSAR project (Jezek, 2003) is plotted over Amery Ice Shelf. The boundaries of the Lambert, Mellor and Fisher flowbands were drawn by tracing the flow directions. Eighteen ice flux gates normal to the velocity vector were placed at intervals of 30 to 40 km for gates 1 to 15, and around 15 km for gates 16 to 18 over the flowbands (Fig. 2).

The study area (original projection is Polar Stereographic) was finally re-projected to the Lambert Azimuthal-equal area to calculate the area values. The total grounded area of Lambert, Mellor and Fisher glaciers is 97,0610 km^2, which is about 4 percent larger than that reported by Rignot (2002) due possibly to the different projections.

3 Previous Mass budget and Basal Flux Studies

Fricker *et al.* (2000b) briefly summarized the previous mass balance studies in the interior basin (the Lambert Glacier drainage basin, LGDB) of the LAS, which is a part of the system that drains through the major ice streams entering the rear of the Amery Ice Shelf. Previous studies inclined to a largely positive mass imbalance for the interior drainage basin, e.g., Allison (1979) estimated mass fluxes for the LGDB, obtaining a overall positive imbalance for the interior (upstream of the GL line, Fig.1) of approximately 30 Gt a^{-1} (50% of total net accumulation), and a positive mass balance of 12 Gt a^{-1} between the grounding line and the GL line; Bentley and Giovinetto (1991) obtained a positive mass imbalance of 39 Gt a^{-1} (78% of total net accumulation) for the entire LGDB though McIntyre (1985) re-assessed the mass balance of the LGDB and suggested a positive mass balance for the interior basin (+2 Gt a^{-1}) and error limits which fell below zero by re-definition of the basin and reinterpretation of surface accumulation based on satellite imagery. Fricker *et al.* (2000b) estimated the total integrated mass flux across the ANARE LGB line, obtaining an ice flux of 44 Gt a^{-1}, which was derived from the observations along the LGB traverse line between LGB05 and LGB69 with an assumed surface velocity factor of 0.87. They also assessed the mass balance of the region between the LGB and GL lines with six different accumulation distributions, with four of the estimates exceeding +30%, which strongly suggested that the mass balance of the region between the two lines is positive. New grounding line of the Lambert Glacier drainage basin was defined using InSAR, which resulted in the mass balance estimate of the basin close to balance (Rignot, 2002). It means prior-determined, largely positive mass imbalances for LGDB are due to incorrect localization of the grounding line. Mass losses between the new and old grounding lines were accounted for in prior estimations of the mass budget of this glacier system. The mass imbalance anomalies upstream the GL line (Allison, 1979; Fricker *et al.*, 2000b), however, can still not be explained by the new mapping of the grounding line location.

Basal melting and freezing beneath the Amery Ice Shelf have been investigated over last five decades by means of field measurements (e.g., Budd *et al.*, 1982; Wong *et al.,* 1998), ice core drilling (Morgan, 1972), modeling (Hellmer and Jacobs, 1992; Williams *et al.,* 2001; Hellmer, 2004) etc. Freezing of up to 0.6 m a^{-1} has been reported for the Amery Ice Shelf, supported by a thick layer of basal marine ice at the "G1" drill site near

69º27'S, 71º42'E and the glaciological mass balance calculations (Morgan, 1972; Budd *et al.*, 1982). Recently, this has been confirmed by the work of Fricker *et al.* (2001), who have mapped accreted marine ice beneath the Amery Ice Shelf. The thickness distribution of the marine ice, predicted to be up to 190 m thick in places, was estimated from the hydrostatic anomaly. An access hole through the shelf drilled by ANARE at AM01 (69º26.5'S, 71º25.0'E) in 2001/02 and a ice core recovered nearby by CHINARE (Chinese Antarctic Expedition) in 2002/03 field season suggested the marine ice layer there is up to 200 m. Estimates based on InSAR data yield local melt rates of 31-32±5 m ice a^{-1} near the southern grounding line (Rignot, 2002; Rignot and Jacobs, 2002). Using hydrographic observations collected near the front of the Amery Ice Shelf, Wong *et al.* (1998) estimated that the amount of ice being lost from the bottom of the Amery Ice Shelf ranged between 10.7 Gt a^{-1} and 21.9 Gt a^{-1}. Hellmer and Jacobs (1992) modeled the sub-Amery ocean thermohaline circulation as a channel flow with seasonal forcing, which indicated a mean melting rate as high as 0.65 m a^{-1} for this ice shelf, equal to the removal of 23 Gt a^{-1} of basal ice. Williams *et al.* (2001) used a three-dimensional numerical ocean model to simulate the ocean cavity beneath the Amery Ice Shelf with two different boundary conditions. The two simulations gave net melt rates of 5.8 Gt a^{-1} and 18.0 Gt a^{-1} respectively. Both models showed basal freezing of several Gt a^{-1}. Hellmer (2004) also reported a spatial average basal melting of 0.35 m ice a^{-1}, and the total basal mass loss of 17.65 Gt a^{-1} beneath the Amery Ice Shelf, being modeled using a coupled ice-ocean model.

4 Data Sets and Methodology

The data sets we used in this study include the MAMM InSAR velocity data (Jezek, 2002; 2003), the RADARSAT-1 Antarctic Mapping Project (RAMP) image mosaic (Jezek, 1999), OSU-DEM (Liu and Jezek, 1999), ICESat GLAS (Geoscience Laser Altimeter System) laser altimeter data (Zwally *et al*., 2003), AIS-DEM (Fricker *et al.*, 2000a), ANTARCTIC ATLAS-DEM (Herzfeld, 2004), BEDMAP ice thickness (Lythe *et al.*, 1999), Surface accumulation data sets by Vaughan *et al.* (1999) and Giovinetto (Giovinetto and Zwally (2000), modified, Giovinetto) (hereafter, Vaughan and Giovinetto

compilations respectively), velocity ratio derived from a model simulation of the ice sheet (Huybrechts, 2002), and in situ measurements collected by the ANARE and CHINARE.

Three approaches have been used to determine the mass balance of Antarctic glaciers, all with their own advantages and limitations (Rignot and Thomas, 2002). The approach considered here is commonly referred to as the mass-budget (Rignot, 2002), or component (flux) (The ISMASS Committee, 2004) method in which the input and output fluxes are individually measured or estimated, and mass budget is determined by the differences between the total input for each catchment area and the corresponding ice flux through the traverse line or the grounding line. The basal melting and freezing rates are estimated assuming mass conservation and steady-state conditions between the gates placed over the flowbands of Lambert, Mellor and Fisher glaciers, similar to the method used by Rignot and Jacobs (2002).

4.1 MAMM InSAR Velocity Products

The principal objective of the MAMM project that occurred during the fall of 2000 is to obtain surface velocities on the ice sheet (Jezek, 2003). MAMM acquired data from about 80ºS latitude to the Antarctic coast, with three times in descending orbit mode and three times in ascending orbit mode. Ice velocity was then measured interferometrically combining ascending and descending passes to obtain a vector measurement of ice velocity (Joughin *et al.*, 1998). This technique has an inherent precision of a couple of meters per year, in practice better than 10 m a^{-1} (Rignot, 2002). The velocity data in vector form from the MAMM were densely produced with a spacing interval of 400 m.

Some patches have no velocity data due to some gaps of RADARSAT SAR image or weak coherence between the pair of images used for InSAR velocity mapping, and kriging was applied to make up these patches (Fig. 3).

Figure 3

4.2 DEMs

DEMs are used to convert to ice thickness that is needed to estimate the ice fluxes, but not available in some regions, assuming hydrostatic equilibrium. There are almost no ice radar thickness data available along the southern grounding line. Over the northern portion of the flowbands where the marine ice accretes onto the base of the shelf, and the airborne radio-echo sounding (ERS) measurement is only to the meteoric-marine ice because the ERS signal does not penetrate the marine ice.

For the purpose of improving the basal flux estimate, three DEMs covering the Amery Ice Shelf, generated based on the European Remote Sensing Satellite (ERS-1) radar altimeter data with different data processing and interpolation, are used in our analysis. The AIS-DEM and ANTARCTIC-ATLAS DEM, with different horizontal resolutions, are interpolated onto the same grid size (400 m cell-size grid) as the InSAR velocity mapping and the OSU-DEM. The OSU-DEM with 400m cell size grid has a vertical accuracy better than 2 m for the central portion of the Amery Ice Shelf (Liu *et al.*, 1999). The AIS-DEM (1 km grid), with a RMS error of 1.7 m in the AIS-DEM heights (Fricker *et al.*, 2000a), is bilinearly resampled to 400 m cell size grid. On the flat Amery Ice Shelf, the error of the ANTARCTIC ATLAS-DEM (3 km grid) is mostly below 3 m (Herzfeld, 2004), which was interpolated and exported to 400 m by 400 m grid using kriging.

In addition, the fourth DEM, created in this study based on the ICESat GLAS data, is used for ice flux calculation across the southern grounding line and gates 1 and 2 (Fig. 2).

An attempt to use the OSU-DEM, AIS-DEM and ANTARCTIC ATLAS-DEM that have similar pattern and errors, to infer an available ice thickness dataset was unsuccessful due to relatively large errors in some sections along the grounding line, so the ICESat GLAS data (version 18 data from L1 and L2a) are used to generate an improved DEM for the southern grounding line region (Zwally *et al.,* 2003).

The ICESat GLAS data have a sensor footprint of 75 m, a typical along-track spacing between footprints of 175 m on ground and an across-track separation of around 10-15 km, which shares the same distribution properties with many other geographical or geological data from surveys that are carried out from vehicles that follow tracks, i.e., the data are densely sampled along track while the flight tracks themselves are widely spaced. Such a distribution poses serious difficulties for most interpolation techniques and results

in a directional bias in the grid (Lythe *et al.,* 2001). To counter this, we conducted a data reduction processing so as to have the new data points spaced larger than 2000 m. Then the cokriging was applied to create a continuous surface (GLAS-DEM) with the OSU-DEM as another variable assuming it has a correct elevation trend though the errors are relatively large around the southern grounding line of the Amery Ice Shelf.

4.3 Ice Thickness

4.3.1 BEDMAP Ice Thickness

Ice thickness data of 159,871 points over the Amery Ice Shelf and neighbor regions, measured by Australian and Russian Antarctic expeditions using airborne radio echo sounding (RES), ground-based RES, and seismic reflection & gravity since 1950's, were downloaded from the BEDMAP website (http://www.antarctica.ac.uk/aedc/bedmap/) (lythe *et al.*, 2001). After cross-validation, 1375 ice thickness data of Mission-ID 8 collected by ANARE in 1968 and 1970/71 using ground-based RES were excluded due to large bias with neighbor data. The ice thickness data were then interpolated onto 400 cell-size grid using kriging.

4.3.2 Column-Averaged Ice Density and Ice Thickness Derived Assuming Hydrostatic Equilibrium

Fricker *et al.* (2001) presented the column-averaged ice density over the Amery Ice Shelf, which was derived from a density model that has two layers of meteoric ice to account for a firn layer plus a marine ice layer at the base of the shelf. Here we also used the density of 921 kg m^{-3} near the grounding line, which was essentially inferred from ice temperature. In 2000/01 and 2001/02, two access holes through the shelf were drilled by a hot-water drilling system at two sites: AM02 (69º42.8'S, 72º38.4'E), located ~ 80 km south of the calving front, where the ice shelf is 373 m thick; and AM01 (69º26.5'S, 71º25.0'E), located ~ 50 km west of AM02, and ~ 100 km from the floating ice shelf edge (Fig. 2). At AM01, the shelf is 479 m thick, the lower 200 m of which is marine ice (Hemer and Harris, 2004). The column-averaged densities at these two sites, 904.7 kg m^{-3} and 899.5 kg m^{-3} at AM01 and AM02 respectively, are deduced using seawater density of 1028 kg m^{-3} (Wong *et al.,* 1998) and the average elevations from three DEMs and the

GPS elevation data nearby. A column-averaged density of 885 kg m^{-3} is also obtained from a 300-meter ice core recovered at a site about 300m away from AM01 assuming the whole marine ice density is equal to the average density of the marine ice at the bottom 25 m of the ice core. Two reasons possibly result in this smaller density value, first, some part of the ice core might be broken during the core drilling, but it was assumed to be integrated when the dimensions were measured in situ. Second, the bottom 25-meter marine ice density (913 kg m^{-3}) was used as the average density of the whole marine ice (200 m thick), which perhaps is also a little smaller than the actual density because the density of marine ice could become larger with depth due to the increase of salinity. The density in this region should, therefore, be around 890-900 kg m^{-3}. First, we generated three density models on 400 m grid by linearly interpolating the density 921 kg m^{-3} at the southern grounding line and 890, 895, 900 kg m^{-3} at AM01 respectively. Three ice thickness maps are obtained by converting the AIS-DEM using these three density models. Three distributions of marine ice beneath the Amery Ice shelf are then derived by subtracting the Russian ice radar data, in the same manner as Fricker *et al*. (2001). The RES records show strong basal echoes under the eastern side (south 71.3º) and under the southern ice shelf (Fricker *et al.*, 2001), which implies basal melting there. Comparing the three marine ice distribution maps, we suggested the density of 895 kg m^{-3} at AM01 should be reasonable. At last, the column-averaged ice density distribution is modified approximately along the ice flow direction by minimizing the hydrostatic height anomaly, namely the difference between the measured surface height and the surface height calculated from measured ice thickness (Fricker *et al.*, 2001). The new density distribution includes three portions, 921 km m^{-3} to 914.7 kg m^{-3} between 0 (the southern grounding line) ~ 215 km, 914.7 kg m^{-3} to 903.5 kg m^{-3} between 215~315 km, and 903.5 kg m^{-3} to 890.5 kg m^{-3} from 315 km to the calving front, which approximately passes through AM01 with the density of 895 kg m^{-3}. Column-averaged density decreases linearly within each portion.

Ice thickness (Z) distributions can then be generated from the OSU-DEM, AIS-DEM, ANTARCTIC ATLAS-DEM and the GLAS-DEM surface elevation (H) in an Arc/Info environment, using the above density (ρ_i) distribution, and applied by the hydrostatic equation: $Z = \rho_w H / (\rho_w - \rho_i)$, where ρ_w is the sea-water density of 1028 kg m^{-3}.

4.4 Measured Surface Ice Velocity and Ice Thickness from the LGB Traverse

During 1989-1995, Seventy-three ice-movement stations (LGB00-LGB72) were established along the ANARE LGB traverse route. The stations are typically positioned at 30 km intervals along the traverse route as shown in Figure 1. Across the Lambert Graben the stations have been positioned at intervals of 15 km in order to resolve a more detailed ice velocity in this region. At each station, surface ice-flow velocity magnitude and azimuth were precisely surveyed by GPS in at least two separate years. The mean (2σ) precision of the GPS velocity results is 0.108 m a^{-1}.All but two of these ice-velocity determinations had an estimated accuracy of better than 1 m a^{-1}, and about 60% had an estimated accuracy better than 0.3 m a^{-1} (Kiernan, 2001; Fricker *et al.*, 2000; Manson *et al.*, 2000). Ice thickness was also measured approximately every 10 m along the traverse and averaged over 2 km intervals by a 100 MHz digital ice radar system. The resolution of the individual soundings is about 20 m. In order to supplement radio echo sounding data in some short sections where either poor or no signal returns were obtained, measurements of the local gravity field were taken at 2 km intervals using LaCoste & Romberg Model G gravity meters (Craven *et al.*, 2001).

4.5 Total Accumulation

Following Joughin and Tulzczyk (2002) and Rignot (2002), we estimated integrated accumulation using the average of Vaughan and Giovinetto compilations that were based on essentially the same source data using different analysis and interpolation criteria (Giovinetto and Zwally, 2000).

The total accumulation for each sub-basin is equal to its area multiplied by the annual accumulation rate averaged over the area with the application of GIS techniques. The accumulation totals for the two compilations differ by ~10% upstream and downstream of the ANARE LGB traverse line, which is indicative of the variability introduced by regriding (Joughin and Tulzczyk, 2002). Thus we use a value of 10% for the error in individual glacier drainage accumulation totals, and the catchment area error is assumed to be 5%.

4.6 Ice Fluxes through the ANARE LGB Traverse Line and the Grounding Line

The ice fluxes through the traverse line between adjacent GPS stations are estimated as the product of surface ice velocity, ice thickness, and velocity ratio, equal to column-averaged velocity divided by surface velocity (Thomas *et al.,* 1998, 2000). The velocity was converted into its equivalent value normal to the traverse line (Joughin and Tulaczyk, 2002). Ice velocities were interpolated between adjacent GPS stations, assuming linear change in speed and direction between the two measured values (Wen *et al.*, submitted). Velocity ratio is derived from a model simulation of the Antarctic ice sheet with a 3D thermomechanical ice-sheet model that takes account basal sliding and a variable temperature with depth (Huybrechts, 2002). The ice fluxes for the Lambert, Mellor and Fisher glaciers through the ANARE traverse line were computed as the integral of ice fluxes between the adjacent GPS stations. The errors involved in calculating the total ice discharge include errors in measurements of ice velocity and its direction, ice thickness, and the assumed velocity ratio. We use a value of 5% for the total error in calculated ice-discharge flux, which is consistent with the error analysis by Thomas *et al.* (1998).

The ice flux through the grounding line was estimated as the same method stated above assuming the velocity ratio is equal to 1. The velocity magnitude and azimuth at 400 by 400 m spacing, derived by the MAMM project, are used. The ice thickness ranged from 2000~3000 m along the grounding line was deduced from the GLAS-DEM by a hydrostatic equilibrium equation assuming the densities of column-averaged ice and ocean water are 921 kg m^{-3} and 1028 kg m^{-3} respectively (Fricker *et al.,* 2001; 2002a). The ice thickness derived from the GLAS-DEM still possibly has an uncertainty of 100-200 m in some short sections due to some artifacts derived from the data distribution, potential uncertainty of the geoid and the column-average ice density though the GLAS data themselves are precise. Initial studies have shown that ICESat elevation data are accurate to within ±10 cm (Zwally *et al.*, 2003; Braun *et al.*, 2004). The error of ice velocity is about 5-10 m a^{-1}. Combining the errors of the velocity azimuth and the grounding line location, 10% for the total error is assumed in calculated ice flux across the grounding line.

4.7 Ice Fluxes through the Gates and Basal Fluxes beneath the Flowbands

Ice fluxes through the 18 gates over the flowbands are calculated using the InSAR velocity and ice thickness derived from the BEDMAP project and four DEMs. The mean velocity and ice thickness for the 18 gates over the flowbands are plotted in Fig. 4. Combined the surface accumulation, basal fluxes between two gates can then be estimated. Values are quoted in Gt ice a^{-1} and m ice a^{-1} for ice flux and basal flux respectively using an ice density of 917 kg m^{-3}.

Figure 4

Ice velocity (V_{ij}), thickness (H_{ij}) and width (ΔX_{ij}) were derived from 400 m cell-size grids along the *i*th gate, and ice flux (F_i) across the *ith* gate was calculated as

$$F_i = \sum \left(\frac{V_{ij} H_{ij} + V_{ij+1} H_{ij+1}}{2} \right) \Delta X_{ij} \rho_i$$

*j=1*th, ..., *n-1*th velocity, ice thickness and width measurements. (1)

where ρ_i is column-averaged ice density at the *i*th gate.

Basal melting and freezing rate beneath an area defined by adjacent two gates and the boundaries of the flowbands can be deduced from two gate fluxes F_{i+1}, F_i downstream and upstream, and surface accumulation δ_A , using conservation of mass as

$$\dot{B} = \frac{F_{i+1} - F_i - \delta_A}{\delta A} \qquad (2)$$

where δA is the ice shelf area in between the two gates.

There are several sources of error in our estimate of ice fluxes through the gates and the basal melting and refreezing rates. InSAR velocity has an uncertainty of about 5~10 m a^{-1}, which is very small comparing the average velocity of larger than 300 m a^{-1}at any gates (Fig. 4). The median absolute difference between observed and predicted ice thickness from BEDMAP is 21 m, while the RMS error of the jackknife resample is 101 m over Amery Ice Shelf (Lythe *et al.*, 2001). Fricker *et al.* (2001; 2002a) presented that the error in ice thicknesses interpolated across the southern portion has an upper limit of

~200 m while the RMS of ice thickness differences at intersections of RES flight lines in the northwest part of the shelf is 26 m. It implies the uncertainty of measured thickness is less than 8%. The uncertainty of ice thickness originated from DEMs includes the errors from the DEM heights, column-averaged ice density and geoid model. Surface heights from three DEMs have an uncertainty of within ±3 m. The density model has an uncertainty of 5 kg m^{-3}, which is consistent with the error analysis by Fricker *et al.* (2002a). The geoid height fields may have errors of up to 3 m as evidenced by the differences taken between two geopotential models (OSU91A and EGM96) (Fricker *et al.,* 2002a). All these errors may give an overall uncertainty up to 40~50 m in ice thickness. Equations (1) and (2) then give maximum errors in F_i and $\dot{B}$ of about 10% and 15% respectively, which are consistent with the swings of F_i and $\dot{B}$ in Fig. 5 and 6.

5 Results

5.1 Mass budgets of the Lambert, Mellor, and Fisher Glaciers

The differences between the accumulation (input) and discharge (output) give the mass budgets for the Lambert, Mellor and Fisher glaciers, upstream and downstream and as a whole. The results with uncertainties are listed in Table 1, 2 and 3 respectively.

Table 1, 2, 3

From Table 1 to 3 several features can be observed. First, Lambert and Mellor glaciers upstream the ANARE traverse line have positive imbalances of 3.9±2.1 Gt a^{-1} and 2.1±2.4 Gt a^{-1} respectively while the Fisher Glacier is approximately in balance. The total ice flux for the three glaciers across the traverse line is 35.2±1.8 Gt a^{-1}, and the total surface accumulation upstream the traverse line is 41.6±4.6 Gt a^{-1}, thus the whole upstream region has a positive imbalance of 5.9±4.9 Gt a^{-1}. Second, The three glaciers downstream the traverse line are in a negative imbalance, specially, the lower elevation region of the Lambert Glacier has a remarkable negative imbalance of -5.0±2.7 Gt a^{-1}. The total ice flux for the three glaciers across the southern grounding line is 54.0±5.4 Gt a^{-1}, and the total input (accumulation plus ice flux across the ANARE traverse line) is

45.5±2.1 Gt a^{-1}, thus the downstream region as a whole has a negative imbalance of -8.5±5.8 Gt a^{-1}. Third, the mass budgets of the Lambert, Mellor, Fisher glaciers are -2.8±3.4 Gt a^{-1}, 1.6±3.0 Gt a^{-1} and -1.3±1.0 Gt a^{-1} , which suggests that the three glaciers are close to balance though Lambert and Fisher glaciers more likely incline towards negative imbalance while the Mellor Glacier trends to be positive imbalance. The whole drainage basin of the three glaciers is also approximately in balance with a mass budget of -2.6±6.5 Gt a^{-1}. Four, the area of the Lambert and Mellor glaciers upstream the traverse line covers 77% of the drainage basin. It means most of the whole drainage basin is perhaps slightly thickening while the downstream portion is thinning.

5.2 Basal Melting and Freezing beneath the Flowbands

The fluxes through the southern grounding line and each gate are plotted in Fig. 5. Ice flux across the grounding line is 58.9±5.9 Gt ice a^{-1}, and around 285 km from the southern extremity of the Amery Ice Shelf at gate 8, it drops to 9.7±1.0 Gt ice a^{-1}, then the ice flux increases due to refreezing, near the ice shelf front, it drops again due to higher melting rate resulted from tidal pumping and the seasonally warmer waters of the coastal current (Jacobs *et al.*, 1992).

Figure 5

The basal melting and freezing rates beneath the three flowbands are plotted in Fig. 6. The mean melting rate is -23.0±3.5 m ice a^{-1} near the southern grounding line, which decreases rapidly downstream, and transits to refreezing at around 300 km from the southern extremity of the ice shelf. Mean freezing rates of the flowbands are around 0.5±0.1 to 1.5±0.2 m ice a^{-1}. The total basal melting is -50.3±5.0 Gt ice a^{-1} (which includes part of the refrozen marine ice). The total marine ice accreted is 7.0±0.7 Gt ice a^{-1}.

Figure 6

6. Discussion

Besides the ANARE LGB traverse, in early 1970's, eleven ice-movement stations were established further downstream of the LGB traverse, which was referred to as GL line by Fricker *et al.* (2000b). The stations at two ends of the GL line are beyond the margin of the Lambert and Fisher glaciers (Fig. 1). In situ measurements of ice velocity and thickness are available to be used in mass-balance estimates. The normal velocity and the thickness distributions were integrated to derive a total mass flux across the line of 29.7 Gt a^{-1} (Allison, 1997), assuming the velocity ratio of 0.8 and a column-averaged ice density of 870 kg m^{-3}, which converted to 33.8 Gt a^{-1} for the velocity ratio of 0.87 and the ice density of 910 kg m^{-3} (Fricker *et al.*, 2000b), and to 36.9 Gt a^{-1} in this study for the velocity ratio of 0.95 derived from a model simulation of the Antarctic ice sheet. Allison (1979) obtained an overall positive imbalance for the interior upstream of the GL line of approximately 30 Gt a^{-1} (50% of total net accumulation). Fricker *et al.* (2000b) suggested that the mass balance of the region between the LGB and GL lines was significantly positive.

Here we define the interior basin upstream the GL line by tracing the flowlines from the RADARSAT mosaic and the steepest path from the OSU-DEM. The area is 940, 820 km^{-2}, which is 13.7% less than the area given by Allison (1979), but larger than the area (902, 000 km^2) reported by McIntyre (1985). The total net accumulation is 51.8 Gt a^{-1}, which is also about 8 Gt a^{-1} less than that reported by Allison (1979).

The region between the LGB and GL lines is delineated by tracing the steepest paths from the two GL line ends. The ice flux across the LGB traverse line into this region is 37.1 Gt a^{-1}, and the total accumulation is 10.3 Gt a^{-1}, which yield a positive imbalance of 28.8% of the total input (ice flux through the LGB line plus the total accumulation in the region). The total accumulation of the Lambert, Mellor and Fisher glaciers downstream the GL line is 1.0 Gt a^{-1}. Comparing the input (ice flux across the GL line plus the total accumulation of the three glaciers downstream the GL line) and output (the ice flux across the grounding line of the three glaciers), we can obtain that the region downstream the GL line has a significant negative imbalance larger than -16.1 Gt a^{-1}, or -42.5% of the total input because the GL line extends beyond the boundaries of Lambert and Fisher

glaciers.

The significant positive imbalances for the interior basin upstream the GL line reported by Allison (1979) and Fricker *et al.* (2000b) are possibly due to overestimate of the total accumulation and/or underestimate of the ice flux through the GL line. The 11 ice-movement stations along the GL line is 50-100 km apart, which may result in relatively larger error for ice flux calculation though Allison (1979) interpolated surface velocities between the GL stations with reference to the ice thickness. The ice flux is more possibly underestimated, which result in strongly negative imbalance downstream the line (comparing with the ice flux across the grounding line in this study) and significant positive imbalance upstream the line.

Our mass budget estimates in this study show the Lambert, Mellor and Fisher glaciers as a whole is close to balance state while the drainage upstream the LGB line (accounts for 82.5% of the three glaciers) has a positive imbalance and downstream the line has a negative imbalance, but the magnitudes are comparatively smaller. Davis *et al.* (2001) estimated surface elevation change (*dH/dt*) using Seasat and Geosat satellite radar altimeter measurements over the East Antarctic Ice Sheet over the period from 1978 to 1988. They obtained the *dH/dt* estimate of -2.3±2.2 cm a^{-1} north 72.1º (the southerly orbit limit of Seasat/Geosat), and the ERS-1/2 *dH/dt* estimate of -1.8±1.7 cm a^{-1} up to 73.5º for 1992 to 1996 computed using a subset of the published data found in Wingham *et al.* (1998) in the LAS. These results show the lower portion of the three glaciers is possibly thinning slightly, and approximately consistent with our analysis in this study which indicates a negative mass budget downstream the LGB line. However, the most recent ERS radar altimetry assessment of elevation change from 1992-2003 indicates moderate thickening south and east of the Amery Ice Sheet in the LAS (Davis *et al.*, 2005). The possible explanations include: (1) Snow accumulation rates vary temporally. The altimetry results are more susceptible to the effects of temporal variability in snow accumulation and snow density (McConnell *et al.*, 2000; Thomas *et al.*, 2001; Davis *et al.*, 2005) while the mass budget estimate using the accumulation data spanning from 1950's to 1990's (Higham *et al.,* 1997) should give a clearer indication of long-term ice sheet behavior (Thomas *et al.*, 2001). (2) The discharge flux through the grounding line is not directly responding to the contemporary accumulation rate.

The boundaries of the three flowbands drawn on the basis of velocity vector data are correlated with those defined tracing linear features, i.e., the dominant foliation trend and medial moraines (Hambrey and dowdeswell, 1994) in the second Antarctic Mapping Mission (MAMM) mosaic (Fricker *et al.*, 2002b) although not exact. For example, Fricker *et al.* (2002b) suggested that the Rift B was between the Fisher and Mellor flowbands, but the boundary between these two flowbands in this study is located in the middle way of Rift B and Rift A at the calving front, which is about 15 km apart. Flow lines (the boundaries of the flowbands) inferred from velocity vectors indicate the present flow in the ice shelf while those drawn on the basis of the foliation trend and medial moraines have been incorporated into the ice over long periods of time; variations between the positions of these two kinds of flow lines should show how ice flow has differed in the past spanning over around 1000 years deduced from the distance and average velocity from the southern grounding line to the calving front, which is similar to the observations revealed by Jezek (1984) on the Ross Ice Shelf. The basal flux estimate in this study, however, is made by assuming that the ice shelf is in a steady state, an assumption supported by surface elevation and velocity data, which show little change between 1968 and the present (Williams *et al.*, 2001; Phillips, 1999).

The total melting of ice discharge (F_M) across the grounding line is estimated as

$$F_M = F_{GL} - F_{IR} + \Phi A \qquad (3)$$

where F_{GL} is ice flux across the southern grounding line, F_{IR}, ice flux derived using Russian ice radar thickness at gate 18, assuming ice radar can't penetrate the marine ice, and the signal is reflected at the meteoric-marine ice boundary; ΦA, total accumulation over the three flowbands. F_M of 43.3 Gt ice a^{-1} is calculated by equation (3), which is equal to 79.6% of the ice across the southern grounding line. If comparing the minimum ice flux of 9.7 Gt ice a^{-1} at gate 8 with the ice flux through the grounding line, we can obtain the total basal melting of ice from the Lambert, Mellor and Fisher glaciers is 49.2 Gt ice a^{-1}, or 83.6% of the ice from interior. From gate 8 the basal melting of the flowbands transits to freezing and the ice from interior loses a little since then. It implies the percentage of the loss of the ice from interior by basal melting beneath the flowbands is about 80% with 5% uncertainty.

Our estimates of the total basal melting, refreezing and net basal mass loss beneath

the three flowbands are 50.3 Gt ice a^{-1}, 7.0 Gt ice a^{-1} and 43.3 Gt ice a^{-1} respectively. The total basal melting and net melting are much larger than the results inferred from modeling (Hellmer and Jacobs, 1992; Williams *et al.*, 2001; Hellmer, 2004) and oceanographic data from Prydz Bay (Wong *et al.,* 1998) for the whole Amery Ice Shelf. The marine ice beneath the three flowbands only covers about one third of the total area which is concentrated in the northwest of the shelf (Fricker *et al.*, 2001). The total basal refreezing beneath the Amery Ice Shelf is, therefore, much larger than 7.0 Gt ice a^{-1} (the total refreezing beneath the three flowbands), and also much larger than the basal freezing of several Gt a^{-1} from modeling (Williams *et al.*, 2001), which forms an accreted ice layer up to 190 m thick and accounts for about 9% of the shelf volume (Fricker *et al.*, 2001). The possible reason for the smaller values derived from oceanography is the small number of 1992 CTD casts across the ice shelf front (Allison, 2003), and much more thorough hydrographic survey was undertaken by ANARE and CHINARE in 2001, 2002 and 2003, which may result in the interaction at the base of the shelf in more detail combining with the data recovered from the access holes through the shelf. The geometry of the ice shelf and the dimensions of the sub-ice cavity play an important role in the modeling of processing occurring beneath the ice shelf, such as basal melting, refreezing, and sub-shelf ocean circulation and tides. Only recently the grounding line of the shelf was defined by hydrostatic equilibrium and InSAR (Fricker *et al.*, 2002a; Rignot, 2002), which result in the Amery Ice Shelf extends ~240 km upstream of the previously reported position. For example, Hellmer and Jacobs (1992) were not able to reproduce the amount of marine ice observed at the 1968 borehole site near G1. With the new substantial extensions of the shelf and the sub-ice cavity the modeling may be able to match our results in this study. Our results indicate that the basal melting, freezing and net melting are much larger than previo.usly thought, and the net basal melting accounts for most of the ice loss of the three glaciers.

Gate 1 is approximately located at the same position of the flux gate located about one glacier-width downstream of the grounding line reported by Rignot (2002) and Rignot and Jacobs (2002). The melting rate between the grounding line and gate 1 is 23.0±3.5 m ice a^{-1} in this study, which is only about two thirds of 31±5 m ice a^{-1} reported by Rignot and Jacobs (2002) though they are still with the uncertainty limits. This is

possibly due to different DEMs used to estimate the ice fluxes across the southern grounding line and gate 1 in two studies. Our estimates of the ice fluxes across the grounding line and gate 1 are 58.9±5.9 Gt ice a^{-1} and 33.7±3.4 Gt ice a^{-1} respectively, corresponding to 57.5±5 Gt ice a^{-1} and 28.4±2 Gt ice a^{-1} reported by Rignot (2002), and the area is 1083 km^2 versus 913 km^2. The ice flux across gate 1 is much larger than that estimated by Rignot (2002).

The spatial distribution of melting and refreezing beneath the three flowbands is similar to the standard conceptual and numerical models in which most melt occurs along the grounding lines (Rignot and Jacobs, 2002), which differs significantly from the results reported by Joughin and Padman (2003). They found that roughly two thirds (54 Gt a^{-1}) of the net melt beneath the Filchner-Ronne Ice Shelf is generated at shallow depths (mean 375 m) near the Ronne Ice Shelf front. Fresh, supercooled water plumes containing platelet crystals have been observed north of the ice front in western Prydz Bay (Penrose *et al.*, 1994). The temperature values immediately below the ice shelf measured by CTD are -2.25 ℃ at AM01 and -2.14 ℃ at AM02 (Leffanue and Craven, 2004). The lower temperature ice shelf water may still be a main control of the melting and freezing processes at the base near the ice shelf front, and may mitigate the melting associated with the tide action.

7 Conclusions

We have estimated the mass budgets of the Lambert, Mellor and Fisher glaciers, and ice fluxes across the gates and the basal melting and freezing beneath the flowbands on Amery Ice Shelf applied to greatly expanded data sets.

Lambert and Mellor glaciers upstream the ANARE LGB traverse line have positive imbalances of 3.9±2.1 Gt a^{-1} and 2.1±2.4 Gt a^{-1} respectively while the Fisher Glacier is approximately in balance. The higher-elevation region as a whole has a positive imbalance of 5.9±4.9 Gt a^{-1}. The three glaciers downstream the LGB traverse line are in a negative imbalance, specially, the lower elevation part of Lambert Glacier has a remarkable negative imbalance of -5.0±2.7 Gt a^{-1}. The downstream region as a whole has a negative imbalance of -8.5±5.8 Gt a^{-1}. The mass budgets of the Lambert, Mellor, Fisher

glaciers are -2.8±3.4 Gt a^{-1}, 1.6±3.0 Gt a^{-1} and -1.3±1.0 Gt a^{-1} , which suggests that the three glaciers are close to balance though Lambert and Fisher glaciers more likely incline towards negative imbalance while the Mellor Glacier trends to be in positive imbalance. The whole drainage basin of the three glaciers is also approximately in balance with a mass budget of -2.6±6.5 Gt a^{-1}. The area of the Lambert and Mellor glaciers upstream the LGB traverse line covers 77% of the whole drainage basin. It means most of the drainage basin is perhaps slightly thickening while the downstream portion is thinning.

The total net accumulation is 51.8 Gt a^{-1} in the interior drainage upstream the GL line, which is 8 Gt a^{-1} less than that reported by Allison (1979). The significant positive imbalances for the interior basin upstream the GL line presented by Allison (1979) and Fricker *et al.* (2000) are possibly due to overestimate of the total accumulation and underestimate of the ice flux through the GL line. The interior basin upstream the GL line is more likely close to balance state or in weak positive imbalance.

Ice flux across the southern grounding line is 58.9 Gt ice a^{-1}, and around 285 km from the southern extremity of the ice shelf, it drops to 9.7 Gt ice a^{-1}, and then the ice flux increases due to refreezing, near the ice shelf front, it drops again due to higher melting. The mean melting rate is -23.0±3.5 m ice a^{-1} near the southern grounding line, which decreases rapidly downstream, and transitions to refreezing at around 300 km from the southern extremity. Mean freezing rates of the flowbands are around 0.5±0.1 to 1.5±0.2 m ice a^{-1}. Our estimates of the total basal melting, refreezing and total basal mass loss beneath the three flowbands are 50.3±5.0 Gt ice a^{-1}, 7.0±0.7 Gt ice a^{-1} and 43.3±4.3 Gt ice a^{-1} respectively. The total basal melting and net melting are much larger than the results inferred from modeling (Hellmer and Jacobs, 1992; Williams *et al.*, 2001; Hellmer, 2004) and oceanographic data from Prydz Bay (Wong *et al.*, 1998) for the whole Amery Ice Shelf. The percentage of the loss of the ice from interior by basal melting beneath the flowbands is about 80±5%. These indicate that the basal melting and freezing are significant components of the mass budget of the Amery Ice Shelf, and active interaction takes place at the ice-ocean interface.

The spatial distribution of melting and refreezing beneath the three flowbands is similar to the standard conceptual and numerical models in which most melt occurs along the grounding lines (Rignot and Jacobs, 2002), which differs significantly from the

results reported by Joughin and Padman (2003).

ACKNOWLEDGEMENTS. This work is supported by the National Natural Science Foundation of China (grants No. 4047128). NASA's Polar Oceans and Ice Sheets Program and NASA Headquarters under the Earth System Science Fellowship Grant (NGT5-30533). We thank M. B. Giovinetto and D. G. Vaughan for providing us with the accumulation compilations, Dejun Tan for providing the ice core density data, especially, M. B. Giovinetto who provided us a new modified accumulation compilation used in this study. Some of the data used within this paper was obtained from the Australian Antarctic Data Centre (IDN Node AMD/AU), a part of the Australian Antarctic Division (Commonwealth of Australia). The data is described in the metadata records "Radio-echo sounding (RES) ice thickness data: LGB traverses 1990-95" Allison, I. (1999) and "Ice sheet surface velocity data: LGB traverses 1989-95" Allison, I. (1999).

References

Allison, I. (1979), The mass budget of the Lambert Glacier drainage basin, Antarctica, *J. Glaciol*., 22(87), 223-235.

Allison, I. (2003), The AMISOR project: ice shelf dynamics and ice-ocean interaction of the Amery Ice Shelf, *FRISP Report*, No. 14.

Bentley, C. R., and M. R. Giovinetto (1991), Mass balance of Antarctica and sea level change. *In* Weller, G., C.L. Wilson and B.A.B. Severin, eds. *International Conference on the Role of the Polar Regions in Global Change: proceedings of a conference held June 11-15, 1990 at the University of Alaska Fairbanks. Vol II.* Fairbanks, AK, University of Alaska. Geophysical Institute/Center for Global Change and Arctic System Research, 481-488.

Berthier, E., B. Raup, and E. Scambos (2003), New velocity map and mass-balance estimate of Mertz Glacier, East Antarctica, derived from Landsat sequential imagery, *J. Glaciol.*, 49(167), 503-511.

Braun, A, K. Cheng, B. Csatho, and C. Shum (2004), ICESat laser altimetry in the Great Lakes, *Proc. Institute of Navigation (ION) 60th ANN. Meeting*, Dayton, Ohio, USA.

Budd, W. F., M. J. Corry and T. H. Jacka (1982), Results from the Amery Ice Shelf project. *Ann. Glaciol.*, 3, 36-41.

Craven, M., M. Higham, and A. Brocklesby (2001), *Ice thickness and surface & bedrock elevations from the Lambert Glacier Basin traverses 1990-1995*. Antarctic CRC Research Report No.23, 1-76. Cooperative Research Centre for Antarctica and the Southern Ocean, University of Tasmania. Horbart.

Davis C. H., R. G. Belu, and G. Feng (2001), Elevation change measurement of the East Antarctic Ice Sheet,

1978-1988, from satellite radar altimetry, *IEEE Trans. Geosci. Remote Sensing*, 39(3), 635-644.

Davis, C.H., Y. Li, J.R. McConnell, M.M. Frey, and E. Hanna. 2005. Snowfall-driven growth in East Antarctic Ice Sheet mitigates recent sea-level rise, *Science*, 308, 1898-1901.

Fricker, H. A., G. Hyland, R. Coleman, and N. W. Young (2000a), Digital elevation models for the Lambert Glacier-Amery Ice Shelf system, East Antarctica, from ERS-1 satellite radar altimetry, *J. Glaciol.*, 46(155), 553-560.

Fricker, H. A., R. C. Warner, and I. Allison (2000b), Mass balance of the Lambert Glacier-Amery Ice Shelf system, East Antarctica: a comparison of computed balance fluxes and measured fluxes, *J. Glaciol.*, 46(155), 561-570.

Fricker, H. A., S. Popov, I. Allison, and N. Young (2001), Distribution of marine ice beneath the Amery Ice Shelf, *Geophys. Res. Lett.*, 28(11), 2241–2244.

Fricker, H. A., I. Allison, M. Craven, G. Hyland, A. Ruddell, N. Young, R. Coleman, M. King, K. Krebs, and S. Popov (2002a), Redefinition of the Amery Ice Shelf, East Antarctica, grounding zone, *J. Geophys. Res.*, 107(B5), 2092, doi:10.1029/2001JB000383.

Fricker H. A., N. W. Young, I. Allison, and R. Coleman (2002b), Iceberg calving from the Amery Ice Shelf, East Antarctica, *Ann. Glaciol.*, 34, 241-246.

Gray, L., N. Short, R. Bindschadler, I. Joughin, L. Padman, P. Vornberger, and A. Khananian (2002), RADARSAT interferometry for Antarctic grounding-zone mapping, *Ann. Glaciol.*, 34, 269-276.

Giovinetto, M.B., and H. J. Zwally (2000), Spatial distribution of net surface accumulation on the Antarctic ice sheet, *Ann. Glaciol.,* 31, 171-178.

Hambrey, M. J., and J. A. Dowdeswell (1994), Flow regime of the Lambert Glacier-Amery Ice Shelf system, Antarctica: structural evidence from Landsat imagery, *Ann. Glaciol.*, 20, 401-406.

Hellmer, H. H., and S. S. Jacobs (1992), Ocean interactions with the base of Amery Ice Shelf, Antarctica, *J. Geophys. Res.*, 97, 20,305-20,317.

Hellmer, H. H. (2004), Impact of Antarctic ice shelf basal melting on sea ice and deep ocean properties, *Geophys. Res. Lett.*, 31, L10307, doi:10.1029/2004GL019506.

Hemer, M., and Harris, P. (2004), Sediments collected from beneath the Amery Ice Shelf, East Antarctica, document sub-ice-shelf circulation of water and sediments throughout the Holocence, *FRISP Report*, No. 15.

Herzfeld, U. C. (2004), *ATLAS OF ANTARCTICA: Topographic Maps from Geostatistical Analysis of Satellite Radar Altimeter Data*. Springer Verlag Heidelberg, New York, Tokyo, 364+XVI pp., 145 maps, 25 gs, 5 tables, 1 chart, CDROM.

Higham, M., M. Craven, A. Ruddell, and I. Allison. 1997. Snow-accumulation distribution in the interior of the Lambert Glacier basin, Antarctica, *Ann. Glaciol.*, 25, 412- 417.

Huybrechts, P. (2002), Sea-level changes at the LGM from ice-dynamic reconstructions of the Greenland and Antarctic ice sheets during the glacial cycles, *Quaternary Science Reviews*, 21 (1-3), 203-231.

The ISMASS Committee. 2004. Recommendations for the collection and synthesis of Antarctic Ice Sheet mass balance data, *Global and Planetary Change*, 42, 1-15.

Jacobs, S. S., H. H. Helmer, C. S. M. Doake, A .Jenkins, and R. M. Frolich (1992), Melting of ice shelves and the mass balance of Antarctica, *J. Glaciol.*, 38(130), 375-387.

Jacobs, S. S., H. H. Hellmer, and A. Jenkins (1996), Antarctic ice sheet melting in the Southeast Pacific, *Geophys. Res. Lett.*, 23(9), 957-960, 10.1029/96GL00723.

Jenkins, A., and C. S. M. Doake (1991), Ice-ocean interaction on Ronne Ice Shelf, Antarctica, *J. Geophys. Res.*, 96(C1), 791–813.

Jezek, K. C. (1984), Recent changes in the dynamic condition of the Ross Ice Shelf, Antarctica, *J. Geophys. Res.,* 89 (B1), 409-416.

Jezek, K.C (1999), Glaciological properties of the Antarctic ice sheet from RADARSAT-1 synthetic aperture radar imagery, *Ann. Glaciol*., 29, 286-290.

Jezek, K. C. (2002), RADARSAT-1 Antarctic mapping project: change-detection and surface velocity campaign, *Ann. Glaciol.,* 263-268.

Jezek, K. C. (2003), Observing the Antarctic Ice Sheet using the RADARSAT-1 synthetic aperture radar, *Polar Geography*, 27(3), 197-209.

Joughin, I.R., R. Kwok, and M.A. Fahnestock (1998), Interferometric estimation of three-dimensional ice-flow using ascending and descending passes, *IEEE Trans. Geosci. Remote Sensing*, GE-36 (1), 25-37.

Joughin, I., and S. Tulaczyk (2002), Positive mass balance of the Ross ice streams, West Antarctica, *Science*, 295(5554), 476-480.

Joughin, I., and L. Padman (2003), Melting and freezing beneath Filchner-Ronne Ice Shelf, Antarctica, *Geophys. Res. Lett.*, 30(9), 1477, doi:10.1029/2003GL016941.

Kiernan, R (2001), *Ice sheet surface velocities along the Lambert Glacier Basin traverse route*. Antarctic CRC Research Report No.23, 1-76. Cooperative Research Centre for Antarctica and the Southern Ocean, University of Tasmania. Hobart.

Leffanue H., and M. Craven (2004), Circulaition and water masses from current meter and T/S measurements at the Amery Ice Shelf, *FRISP Report*, No. 15.

Liu, H., K. C. Jezek, and B. Li (1999). Development of an Antarctic digital elevation model by integrating cartographic and remotely sensed data: A geographic information system based approach, *J. Geophys. Res.*, 104(B10), 23199-23214.

Lythe, M. B., D. G. Vaughan, and the BEDMAP Consortium (2001). BEDMAP: A new ice thickness and subglacial topographic model of Antarctica, *J. Geophys. Res.*, 106(B6), 11,335-11,351.

Manson, R., R. Coleman, P. Morgan and M. King (2000), Ice velocities of the Lambert Glacier from static GPS observations, *Earth Planets Space*, 52, 1031-1036.

McConnell, J. R., R. J. Arthern, E. Mosley-Thompson, C. H. Davis, R. C. Bales, R. Thomas, J. F. Burkhart, and J. D. Kyne (2000), Changes in Greenland ice sheet elevation attributed primarily to snow

accumulation variability, *Nature*, 406, 877-879.

McIntyre, N. F. (1985), A re-assessment of the mass balance of the Lambert Glacier drainage basin, Antarctica, *J. Glaciol*., 31(107), 34-38.

Morgan, V. I. (1972), Oxygen isotope evidence for bottom freezing on the Amery Ice Shelf, *Nature*, 238, 393-394.

Penrose, J., M. Conde, and T. Pauly (1994), Acoustic detection of ice crystals in Antarctic waters, *J. Geophys. Res.*, 99 (C6), 12,573-12,580.

Phillips, H. A. (1999), *Applications of ERS satellite radar altimetry in the Lambert Glacier-Amery Ice Shelf system, East Antarctica*, Ph. D. thesis, 308pp., Univ. of Tasmania, Hobart, Australia.

Rignot, E (2002), East Antarctic glaciers and ice shelves mass balance from satellite data, *Ann. Glaciol.*, 2002, 34, 228-234.

Rignot, E., and S. S. Jacobs (2002), Rapid bottom melting widespread near Antarctic Ice Sheet grounding lines, *Science*, 296, 2020-2023.

Rignot, E., and R. H. Thomas (2002), Mass balance of polar ice sheets. *Science*, 297, 1502-1506.

Thomas, R.H., B.M. Csathó, S. Gogineni, K.C. Jezek and K. Kuivinen (1998), Thickening of the western part of the Greenland ice sheet, *J. Glaciol.*, 46(155), 653-658.

Thomas, R., T. Akins, B. Csatho, M. Fahnestock, P. Gogineni, C. Kim and others (2000), Mass balance of the Greenland ice sheet at high elevations, *Science,* 289(5478), 426-428.

Thomas, R., B. Csatho, C. Davis, C. Kim, W. Krabill, S. Manizade, J. McConnell, and J. Sonntag (2001), Mass balance of higher-elevation parts of the Greenland ice sheet, *J. Geophys. Res.*, 106(D24), 33,707–33,716.

Vaughan, D.G., J.L. Bamber, M.B. Giovinetto, J. Russell, and A.P.R. Cooper (1999), Reassessment of net surface mass balance in Antarctica, *J. Climate*, 12(4), 933-946.

Wen, J., K. C. Jezek, A. J. Monaghan, Sun, B., Ren, J., and P. Huybrechts (2006), Accumulation variability and mass budgets of the Lambert Glacier-Amery Ice Shelf system at high elevations, *Ann. Glaciol.*, 43., submitted.

Whillans, I. M., and R. A. Bindschadler (1998), Mass balance of Ice Stream B, West Antarctica, *Ann. Glaciol.*, 11, 187-193.

Williams, M. J. M., K. Grosfeld, R. C. Warner, R. Gerdes, and J. Determann (2001), Ocean circulation and ice-ocean interaction beneath the Amery Ice Shelf, Antarctica, *J. Geophys. Res.*, 106(C10), 22,383–22,400.

Wingham, D. J., A. J. Ridout, R. Scharroo, R. J. Arthern, and C. K. Shum (1998), Antarctic elevation change from 1992-1996, *Science*, 282, 456-458.

Wong, A. P. S., N. L. Bindoff, and A. Forbes (1998), Ocean-ice shelf interaction and possible bottom water formation in Prydz Bay, Antarctica, *in Ocean, Ice, and Atmosphere: Interactions at the Antarctic*

Continental Margin, Antarct. Res. Ser., vol. 75, edited by S. S. Jacobs and R. F. Weiss, pp. 173-187, AGU, Washington, D. C.

Wu, X., and K. C. Jezek (2004), Antarctic ice-sheet balance velocities from merged point and vector data, *J. Glaciol.,* 2004, 50(169), 219-230.

Zwally, H. J., B.Schutz, W.Abdalati, J. Abshire, C. Bentley, A. Brenner, J. Bufton, J. Dezio, D. Hancock, D. Harding, T. Herring, B. Minster, K. Quinn, S. Palm, J. Spinhirne, and R. Thomas (2002), ICESat's laser measurements of polar ice, atmosphere, ocean, and land, *Journal of Geodynamics*, 34 (3-4), 405-445.

Zwally, H. J., R. Schutz, C. Bentley, J. Bufton, T. Herring, J. Minster, J. Spinhirne, and R. Thomas (2003), *updated current year. GLAS/ICESat L2 Antarctic and Greenland Ice Sheet Altimetry Data V018, 15 October to 18 November 2003*. Boulder, CO: National Snow and Ice Data Center. Digital media.

Table 1. Accumulation, ice fluxes and mass budgets for the Lambert, Mellor and Fisher glaciers upstream the ANARE LGB traverse.

Drainage	Area km^2	Average accumulation rate kg m^{-2} a^{-1}	Accumulation Gt a^{-1}	Ice Flux across traverse Gt a^{-1}	Net budget Gt a^{-1}
Lambert	373,920	52.3	19.5±2.2	17.4±0.9	2.1±2.4
Mellor	373,370	47.5	17.8±2.0	13.9±0.7	3.9±2.1
Fisher	53,560	70.0	3.8±0.4	3.9±0.2	-0.1±0.5
Total	800,850	51.2	41.0±4.6	35.2±1.8	5.9±4.9

Table 2. Accumulation, ice fluxes and mass budgets for the Lambert, Mellor and Fisher glaciers downstream the ANARE LGB traverse.

Drainage	Area km^2	Average accumulation rate kg m^{-2} a^{-1}	Accumulation Gt a^{-1}	Ice Flux across traverse Gt a^{-1}	Total Input[(1)] Gt a^{-1}	Ice Flux Across Grounding line Gt a^{-1}	Net budget Gt a^{-1}
Lambert	51,000	59.8	3.1±0.3	17.4±0.9	20.5±0.9	25.4±2.5	-5.0±2.7
Mellor	75,220	63.0	4.7±0.5	13.9±0.7	18.6±0.9	20.9±2.1	-2.3+2.3
Fisher	43,530	59.5	2.6±0.3	3.9±0.2	6.5±0.4	7.7±0.8	-1.2+0.8
Total	169,750	61.1	10.4±1.2	35.2±1.8	45.5±2.1	54.0±5.4	-8.5±5.8

[(1)] Equal to accumulation plus ice flux across the ANARE LGB traverse line.

Table 3. Accumulation, ice fluxes and mass budgets for the Lambert, Mellor and Fisher glaciers.

Drainage	Area km^2	Average accumulation rate kg m^{-2} a^{-1}	Accumulation Gt a^{-1}	Ice Flux Across Grounding line Gt a^{-1}	Net budget Gt a^{-1}
Lambert	424,930	53.2	22.6±2.3	25.4±2.5	-2.8±3.4
Mellor	448,590	50.1	22.5±2.3	20.9±2.1	1.6±3.0
Fisher	97,090	65.3	6.3±0.6	7.7±0.8	-1.3±1.0
Total	970,610	53.0	51.4±3.6[(1)]	54.0±5.4	-2.6±6.5

[(1)] Error is determined assuming 5% for the average accumulation rate and 5% for the area.

Figure 1. Map of the LAS, showing the location of the Lambert, Mellor and Fisher glaciers (in light grey) and their flowbands (in dark grey), and GPS stations (dot) along the ANARE LGB traverse route and the ice movement stations (diamond) along the GL line. Elevation contours are shown as dashed lines with a 1000 m interval.

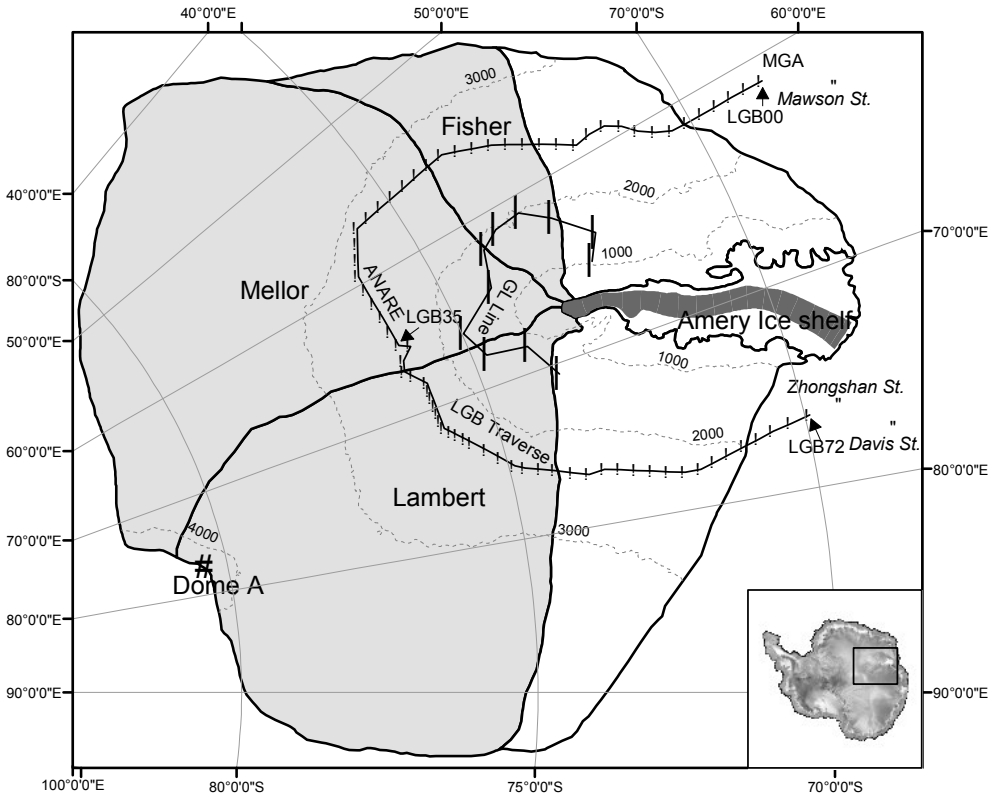

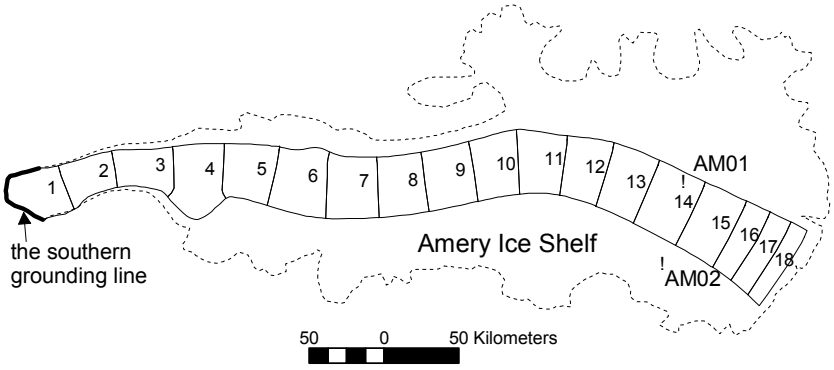

Figure 2. A sketch showing the ice flux gates and their number placed over the flowbands on the Amery Ice Shelf, the southern grounding line (thick line) , i.e., the grounding line of Lambert, Mellor, Fisher glaciers at the rear of the ice shelf, the locations of two access holes (AM01 and AM02) , and the margin of the ice shelf (dash line).

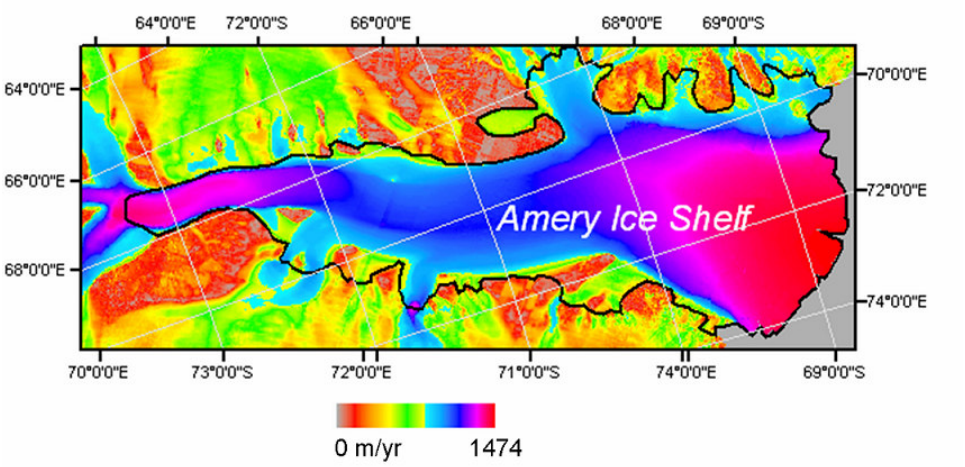

Figure 3. Ice velocity for the Amery Ice Shelf and its neighborhood determined by the MAMM InSAR velocity mapping.

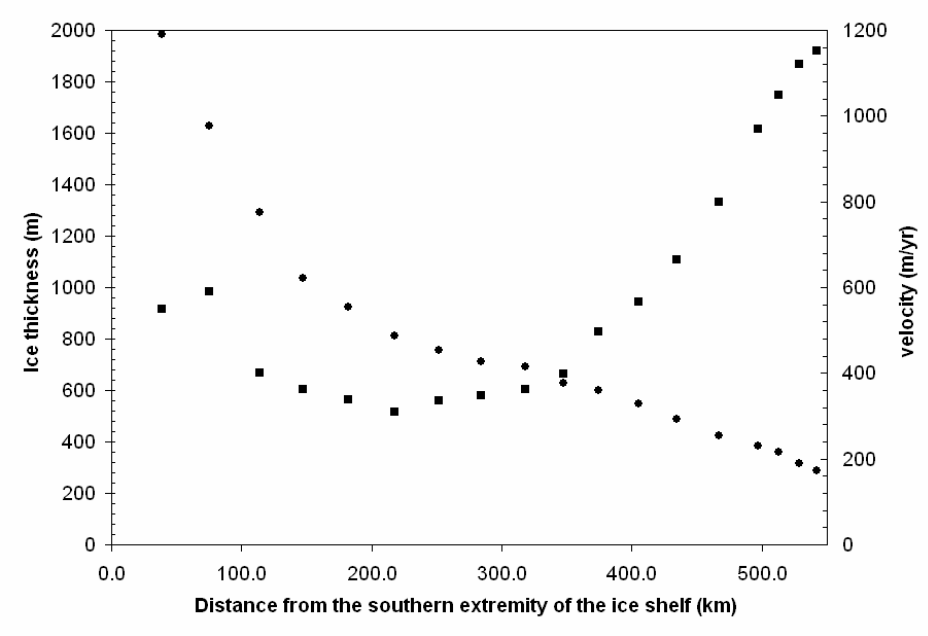

Figure 4. Mean thickness (dot) and ice velocity (square) for the 18 ice flux gates over the flowbands on the Amery Ice Shelf.

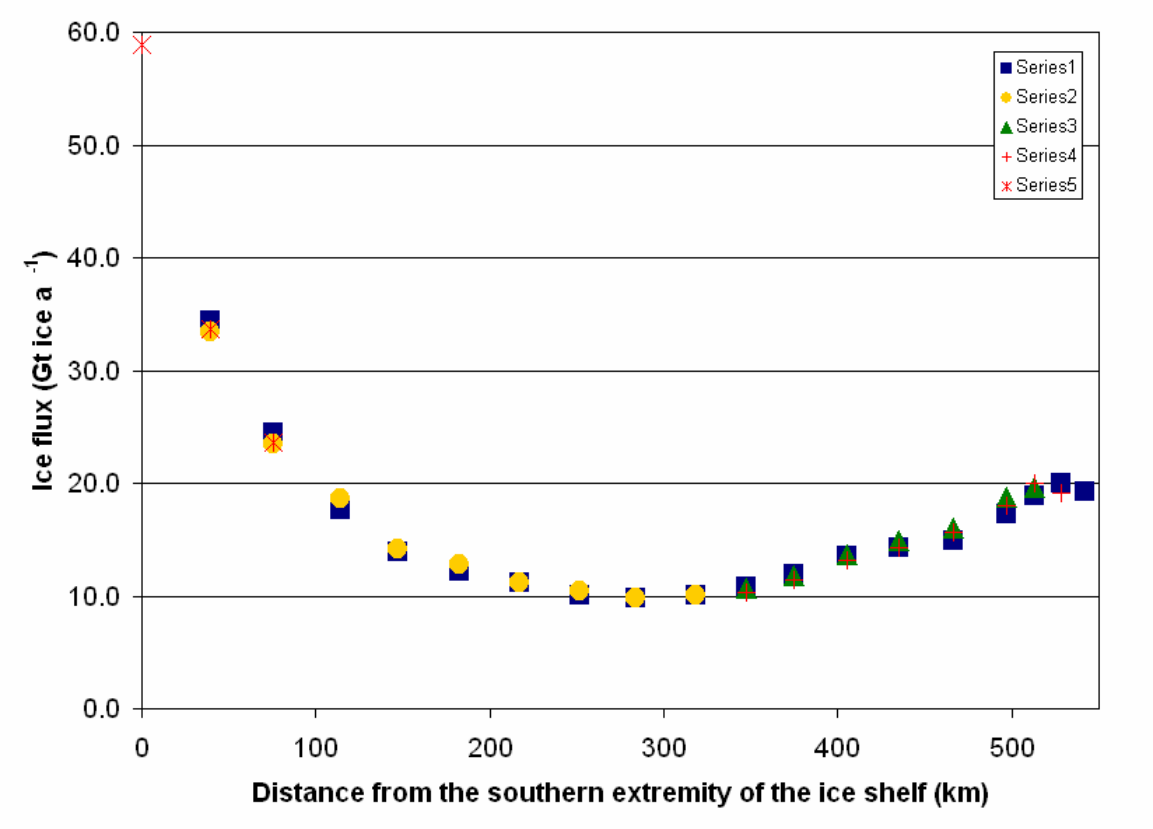

Figure 5. Ice fluxes across the gates over the flowbands on the Amery Ice Shelf. Series 1: derived from AIS-DEM, 2: BEDMAP, 3: ANTARCTIC ALTAL-DEM, 4: OSU-DEM5, 5: GLAS-DEM.

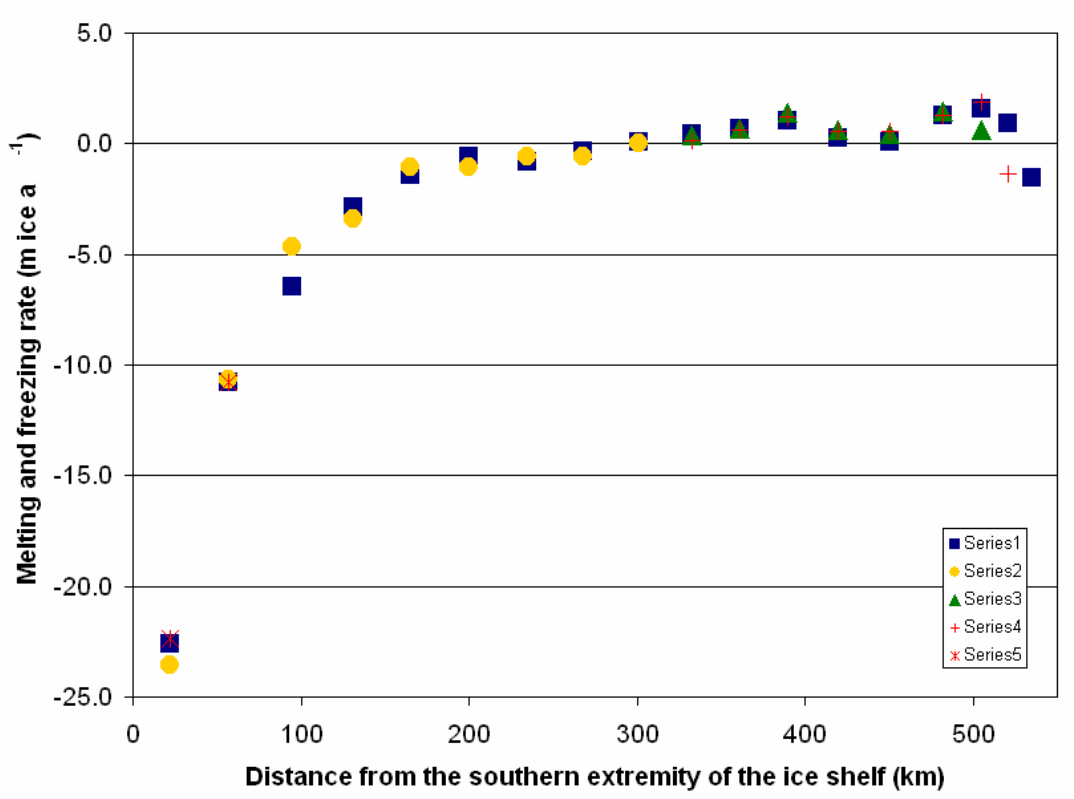

Figure 6. Basal melting and freezing rates beneath the flowbands on the Amery Ice Shelf. Series 1: derived from AIS-DEM, 2: BEDMAP, 3: ANTARCTIC ALTAL-DEM, 4: OSU-DEM5, 5: GLAS-DEM